nature photonics

SUPPLEMENTARY INFORMATION

https://doi.org/10.1038/s41566-019-0493-4

In the format provided by the authors and unedited.

Demonstration of 4.8×10^{-17} stability at 1 s for two independent optical clocks

E. Oelker[1]*, R. B. Hutson[1], C. J. Kennedy[1], L. Sonderhouse[1], T. Bothwell[1], A. Goban[1], D. Kedar[1], C. Sanner[1], J. M. Robinson[1], G. E. Marti[1,5], D. G. Matei[2,6], T. Legero[2], M. Giunta[3,4], R. Holzwarth[3,4], F. Riehle[2], U. Sterr[2] and J. Ye[1]*

[1]JILA, National Institute of Standards and Technology and University of Colorado, Department of Physics, University of Colorado, Boulder, CO, USA. [2]Physikalisch-Technische Bundesanstalt, Braunschweig, Germany. [3]Menlo Systems GmbH, Martinsried, Germany. [4]Max-Planck-Institut für Quantenoptik, Garching, Germany. [5]Present address: Department of Molecular and Cellular Physiology, Stanford University, Stanford, CA, USA. [6]Present address: Horia Hulubei National Institute of Physics and Nuclear Engineering, Magurele, Romania. *e-mail: ericoelker@gmail.com; Ye@jila.colorado.edu

Supplementary Information

E. Oelker[1], R. B. Hutson[1], C. J. Kennedy[1], L. Sonderhouse[1], T. Bothwell[1], A. Goban[1], D. Kedar[1], C. Sanner[1], J. M. Robinson[1], G. E. Marti[1,*], D. G. Matei[2,†], T. Legero[2], M. Giunta[3,4], R. Holzwarth[3,4], F. Riehle[2], U. Sterr[2], & J. Ye[1]

[1]JILA, National Institute of Standards and Technology and University of Colorado, Department of Physics, University of Colorado, Boulder, CO 80309, USA.

[2]Physikalisch-Technische Bundesanstalt, Bundesallee 100, 38116 Braunschweig, Germany.

[3]Menlo Systems GmbH, Am Klopferspitz 19a, 82152 Martinsried, Germany.

[4]Max-Planck-Institut für Quantenoptik, Garching, Germany.

*Present address: Department of Molecular and Cellular Physiology, Stanford University, Stanford, CA 94305, USA.

†Present address: Horia Hulubei National Institute of Physics and Nuclear Engineering, Reactorului 30, 077125 Magurele, Romania.

Characterization of the local oscillator and spectral purity transfer

Figs. 6 and 7 depict characterization measurements of the frequency comb and local oscillator described in the Methods section. Table 1 includes the parameter values for the resonant features in the laser noise model given in Eqn. 3 of the Methods section.

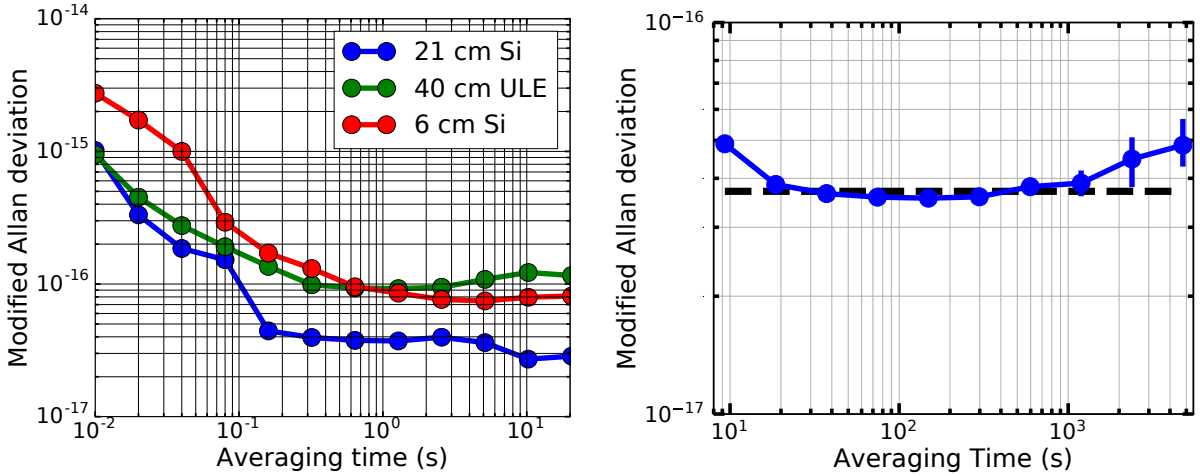

Figure 6 | Left: A three-cornered hat comparison between the local oscillator (21 cm Si) and two reference lasers based on a 6 cm Si cavity operating at 4 K and a 40 cm ULE cavity operating at room temperature characterizes the performance of the local oscillator at short averaging times (<10 s). The data is taken with a zero dead-time Lambda-type frequency counter operating with a 10-ms gate time. **Right:** The typical single-day stability of the local oscillator at longer averaging times is evaluated using the atomic servo correction signal for the 1D Sr lattice clock (30 s servo attack time). The stability is determined by averaging datasets from 13 days that are each at least 20 000 seconds in length after fitting and removing a linear frequency drift from each dataset. On average, the single-day datasets exhibit thermal noise limited stability out to 1000 s, though one dataset showed no departure from thermal noise out to 10 000 s (see Fig 2b). The black dashed line is a flicker frequency noise floor of 3.7×10^{-17} obtained by fitting the Allan deviation between 40-1000 seconds. This is in good agreement with the previously published value of 4×10^{-17}[1]. The error bars represent one standard error confidence intervals.

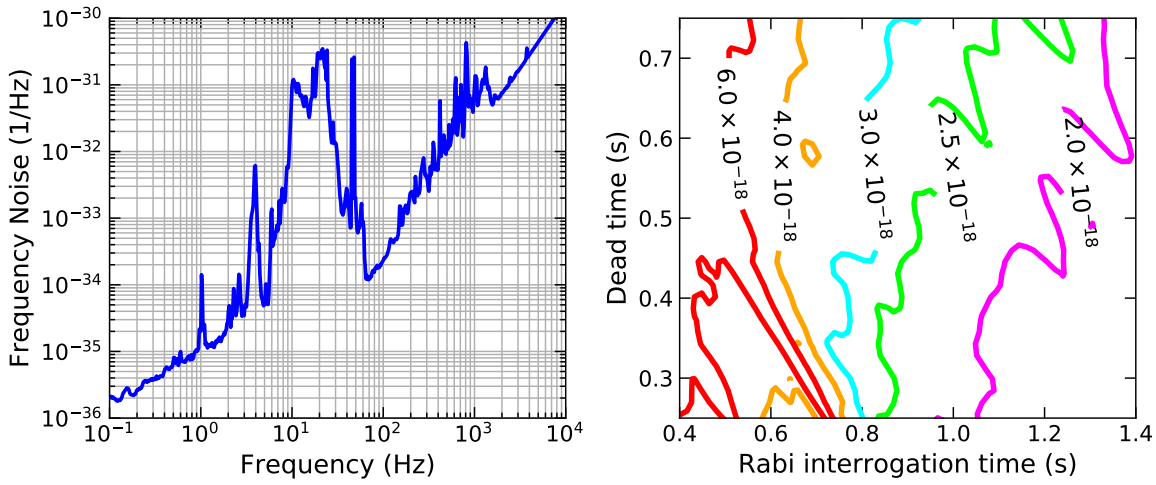

Figure 7 | Estimated instability added to the local oscillator by the optical frequency comb. This is inferred by performing a multi-line comparison measurement against an identical frequency comb [2] in order to characterize the differential noise between their 1542 nm and 698 nm outputs. The two systems are stabilized to a common reference at 1542.14 nm and the heterodyne beat between the systems at 698 nm is recorded. An Allan deviation of this measurement is shown in Fig. 4 in the main text. **Left:** Fractional frequency noise power spectral density of the two-comb 698 nm hetrodyne beat. The accumulated optical phase drift observed over a seven hour measurement is only $1.5 \times 2\pi$, which corresponds to a fractional frequency offset with respect to the 698 nm carrier of 1.3×10^{-19}. The large feature between 5-50 Hz arises due to acoustic noise present at the time of the qualification measurement. Since relocating the system to JILA, the vibrational and acoustic isolation has been improved significantly. By analyzing the three-cornered hat comparison data from Fig. 6 in the frequency domain one infers that this spectral feature has been reduced by at least an order of magnitude since, if present, it would appear to limit the stability of the 40 cm ULE cavity at these Fourier frequencies. **Right:** The contribution from the comb to the Dick effect limit for clock stability is computed by inserting the measured frequency noise power spectral density into Eqn. 2 in the main text. For the operating conditions used here (550-600 ms interrogation time and 570 ms dead time), the comb contribution is negligible.

Table 1 | Eqn. 3 in Methods presents the functional form of the local oscillator noise model. The parameters corresponding to the resonant features in this model are tabulated below.

Index	f_i (Hz)	a_i (1/Hz^3)	Γ_i (Hz)
1	5.7	7.0e-34	1.0
2	12.7	1.5e-34	1.5
3	20.0	4.0e-34	0.1
4	30.0	5.0e-34	0.1
5	40.0	5.0e-34	0.1
6	45.0	1.0e-34	4
7	55.0	4.0e-34	1.2

Magnetic field noise rejection from a four-point locking sequence

As discussed in the main text, fluctuations in the magnetic field background in the laboratory will induce Zeeman shifts in the clock transition due to the presence of nuclear spin in ^{87}Sr. The Zeeman sensitivity for the $|^1S_0, m_F = \frac{9}{2}\rangle \rightarrow |^3P_0, m_F = \frac{9}{2}\rangle$ transition is approximately 490 Hz/G [3], so rapid changes in the magnetic field at the 100 μG level can induce 10^{-16} level frequency excursions in the 1D lattice clock. In the discussion that follows, a frequency-domain treatment of this noise coupling is presented. A similar analysis in the time-domain is available elsewhere in the literature [4].

A measurement of the detuning of the laser from the line center, $\Delta[n]$ where n is the experimental cycle index, will include an additional contribution from the magnetic field background:

$$\Delta[n] = \Delta_{\text{laser}}[n] + \Delta_{\text{field}}[n] \tag{1}$$

For the present discussion all other sources of technical noise are omitted for the sake of simplicity. We make the further simplifying assumption that neither the laser nor the background field exibit long-term drift so we can repeatedly interrogate the clock transition without active feedback. This allows one to neglect the impact of the servo on the frequency

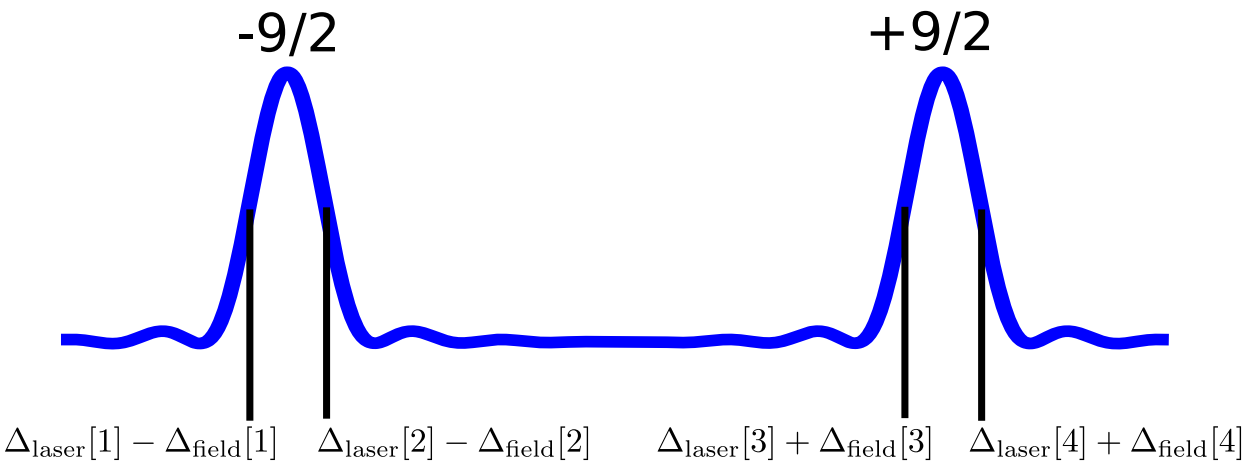

Figure 8 | Diagram depicting the frequency measurements required for a four-point lock in the 1D lattice clock. By averaging these four measurements one may reject frequency noise arising from first-order Zeeman shifts induced by slowly varying magnetic fields in the laboratory.

record of the clock. The purpose of the present discussion is to derive the impact of short term noise from the laser and background field on the clocks frequency record.

To reject the magnetic field noise in the 1D clock, the detuning of the laser from resonance is measured using a four-point spectroscopy sequence as described in the main text. The four point measurement sequence for the 1D lattice clock is depicted in Fig. 8. The important thing to note is that the first-order Zeeman shifts on the $|^1S_0, m_F = \pm\frac{9}{2}\rangle \rightarrow |^3P_0, m_F = \pm\frac{9}{2}\rangle$ transitions will be anticorrelated and should largely cancel when all four measurements are averaged provided that the magnetic field doesn't change dramatically over the course of the measurements (in this work, fluctuations in the second-order Zeeman shift are too small to have a significant impact on the clock stability and are ignored in the present discussion). The discussion that follows also applies to the spectroscopy sequence used in the 3D clock, though in that case Δ_{field} is intrinsically a factor of 22 smaller [3]. These four measurements yield the following

$$\Delta[1] = \Delta_{\text{laser}}[1] - \Delta_{\text{field}}[1] \tag{2}$$

$$\Delta[2] = \Delta_{\text{laser}}[2] - \Delta_{\text{field}}[2] \tag{3}$$

$$\Delta[3] = \Delta_{\text{laser}}[3] + \Delta_{\text{field}}[3] \tag{4}$$

$$\Delta[4] = \Delta_{\text{laser}}[4] + \Delta_{\text{field}}[4] \tag{5}$$

$$\langle \Delta_{\text{laser}} \rangle \approx \frac{1}{4} \left(\Delta[1] + \Delta[2] + \Delta[3] + \Delta[4] \right) \tag{6}$$

where $\langle \Delta_{\text{laser}} \rangle$ denotes the average laser detuning from resonance over the span of all four measurements and the sign convention chosen for Δ_{field} corresponds to the $|^1S_0, m_F = \frac{9}{2}\rangle \rightarrow |^3P_0, m_F = \frac{9}{2}\rangle$ transition. The frequency record for the laser is then estimated by averaging successive four-point measurement cycles

$$\widehat{\Delta}_{\text{laser}} = \left\{ ..., \frac{1}{4} \left(\Delta[1] + \Delta[2] + \Delta[3] + \Delta[4] \right), \frac{1}{4} \left(\Delta[5] + \Delta[6] + \Delta[7] + \Delta[8] \right), ... \right\} \tag{7}$$

In order to understand the impact of laser and field noise on $\widehat{\Delta}_{\text{laser}}$, one can derive transfer functions $H[\omega_m]$ and $G[\omega_m]$ corresponding to the coupling of laser and field noise respectively in the Fourier domain. To this end, it is useful to point out that the sequence in Eqn. 7 can be constructed by applying the following two operations to the laser and field noise.

Step 1: Filter the laser and field noise and add the resulting sequences:

$$\Delta_{\text{filt}}[n] = h * \Delta_{\text{laser}}[n] + g * \Delta_{\text{field}}[n] \tag{8}$$

where $*$ denotes the convolution operator and

$$h[n] = \frac{1}{4}\sum_{k=0}^{3}\delta[n-k] \tag{9}$$

$$g[n] = \frac{1}{4}\left(-\delta[n] - \delta[n-1] + \delta[n-2] + \delta[n-3]\right) \tag{10}$$

are discrete-time filter functions corresponding to the desired transfer functions. This operation yields

$$\begin{aligned}\{...,\Delta[1],\Delta[2],\Delta[3],\Delta[4],\Delta[5],\Delta[6],...\}& \\ \rightarrow \left\{...,\frac{1}{4}\left(\Delta[1]+\Delta[2]+\Delta[3]+\Delta[4]\right),\frac{1}{4}\left(\Delta[2]+\Delta[3]+\Delta[4]+\Delta[5]\right),...\right\}& \\ = \{...,\Delta_{\text{filt}}[4],\Delta_{\text{filt}}[5],...\}&\end{aligned} \tag{11}$$

Step 2. Downsample the data by a factor of four.

$$\begin{aligned}\left\{...,\frac{1}{4}\left(\Delta[1]+\Delta[2]+\Delta[3]+\Delta[4]\right),\frac{1}{4}\left(\Delta[2]+\Delta[3]+\Delta[4]+\Delta[5]\right),...\right\} \rightarrow& \\ \left\{...,\frac{1}{4}\left(\Delta[1]+\Delta[2]+\Delta[3]+\Delta[4]\right),\frac{1}{4}\left(\Delta[5]+\Delta[6]+\Delta[7]+\Delta[8]\right),...\right\} = \widehat{\Delta}_{\text{laser}}&\end{aligned} \tag{12}$$

The impact of both magnetic field noise and laser noise on $\widehat{\Delta}_{\text{laser}}$ can be understood by considering the discrete Fourier transform of the frequency record Δ_{filt} followed by a reduction in bandwidth due to downsampling.

$$\Delta_{\text{filt}}[\omega_m] = H[\omega_m]\Delta_{\text{laser}}[\omega_m] + G[\omega_m]\Delta_{\text{field}}[\omega_m] \tag{13}$$

where $\omega_m = \frac{m\omega_s}{N_s}$, $\omega_s = 2\pi/T_c$ is our sampling rate in angular frequency units, T_c is our experimental cycle time, and N_s is the total number of samples, and $H[\omega_m]$ and $G[\omega_m]$

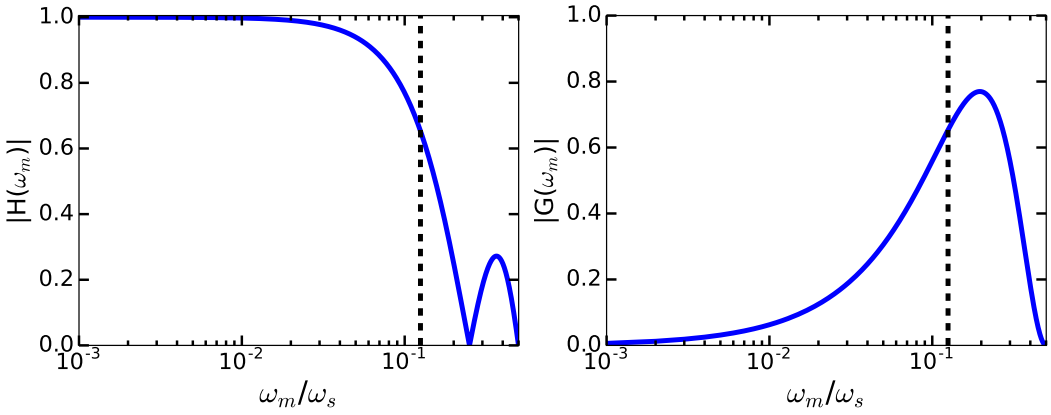

Figure 9 | Transfer functions corresponding to the coupling of laser noise (left) and magnetic field noise (right) to the frequency record of the clock when using the four-point interrogation sequence depicted in Fig. 8. The x-axis is normalized by the clock cycle frequency ω_s. The dashed lines indicate the Nyquist frequency ($\omega_s/8$) after performing the four-point analysis.

denote the discrete Fourier transforms of the filter functions $h[n]$ and $g[n]$ respectively.

$$H[\omega_m] = \sum_{n=0}^{\infty} h[n] e^{-j\omega_m n} = \frac{1}{4} \sum_{k=0}^{3} e^{-j\omega_m k} = \frac{1}{4} \frac{1 - e^{-j4\omega_m}}{1 - e^{-j\omega_m}} = \frac{1}{4} \frac{e^{-j2\omega_m}}{e^{-j\omega_m/2}} \frac{\sin(2\omega_m)}{\sin(\omega_m/2)} \tag{14}$$

$$G[\omega_m] = \frac{1}{4} \left(-1 - e^{-j\omega_m} + e^{-j2\omega_m} + e^{-j3\omega_m} \right) \tag{15}$$

$H[\omega_m]$ and $G[\omega_m]$ are simply transfer functions from laser and magnetic field noise to our frequency record. The magnitudes of both filters are plotted in Fig. 9. We see that $\Delta_{\text{laser}}[\omega_m]$ is effectively low-passed while $\Delta_{\text{field}}[\omega_m]$ is high passed. Therefore, a four-point interrogation sequence will reject magnetic field noise provided that the fluctuations in the field are sufficiently slow. After downsampling the data, the bandwidth of the coupled noise is reduced by a factor of four. The dashed lines in Fig. 9 indicate the Nyquist frequency after downsampling.

Note that, at Fourier frequencies approaching the Nyquist rate, laser and magnetic field induced noise couple to the frequency record with almost equal magnitude. This spectroscopy sequence is therefore not effective at rejecting high frequency magnetic field induced noise

as it is unable to distinguish between the two noise sources.

Along with a reduction in bandwidth, the downsampling of the data by a factor of four leads to an additional aliasing process. One might assume that this would lead to an increase in the Dick effect limit since laser noise at Fourier frequencies $\omega_m = \frac{\omega_s}{4}$ and $\omega_m = \frac{\omega_s}{2}$ will be aliased down to DC. In fact, the Dick effect limit remains the same since $H[\omega_m] = 0$ at these frequencies. $H[\omega_m]$ therefore functions as an anti-aliasing filter. However, $G[\frac{\omega_s}{4}]$ is non-zero, so magnetic field noise at this frequency can alias down to DC and degrade the long-term stability of the clock.

References

[1] Matei, D. G. et al. 1.5 μm lasers with sub-10 mHz linewidth. *Phys. Rev. Lett.* **118,** 263202 (2017).

[2] Giunta, M. Hänsel, W., Fischer, M., Lezius, M., & Holzwarth, R. Sub-mHz spectral purity transfer for next generation strontium optical atomic clocks, in *Conference on Lasers and Electro-Optics.* SM1L.5 (OSA, 2018).

[3] Boyd, M. M. et al. Nuclear spin effects in optical lattice clocks. *Phys. Rev. A.* **76,** 022510 (2007).

[4] Barwood, G.P., Huang, G., King, S.A. Klein, H.A., Gill, P. Frequency noise processes in a strontium ion optical clock. *J. Phys. B: At. Mol. Opt. Phys.* **48**, 035401 (2015).